CONF-871243--4

CONF-871243--4

DE88 005058

A New Look at Reaction Mechanisms with 4π Charged-Particle and Neutron Multiplicity Measurements

D.G. Sarantites, T.M. Semkow, L.G. Sobotka,
V. Abenante, Z. Li, Z. Majka, N.G. Nicolis, and D.W. Stracener

Department of Chemistry, Washington University, St. Louis, Missouri 63130

D.C. Hensley and J.R. Beene

Oak Ridge National Laboratory, Oak Ridge, Tennessee 37830

and

H.C. Griffin

University of Michigan, Ann Arbor, Michigan 48109

MASTER

Invited Talk
Texas A&M University Symposium on Hot Nuclei
College Station, Texas, December 7-10, 1987

DISCLAIMER

This report was prepared as an account of work sponsored by an agency of the United States Government Neither the United States Government nor any agency thereof, nor any of their employees, makes any warranty, express or implied, or assumes any legal liability or responsibility for the accuracy, completeness, or usefulness of any information, apparatus, product, or process disclosed, or represents that its use would not infringe privately owned rights. Reference herein to any specific commercial product, process, or service by trade name, trademark, manufacturer, or otherwise does not necessarily constitute or imply its endorsement, recommendation, or favoring by the United States Government or any agency thereof. The views and opinions of authors expressed herein do not necessarily state or reflect those of the United States Government or any agency thereof.

DISTRIBUTION OF THIS DOCUMENT IS UNLIMITED

A New Look at Reaction Mechanisms with 4π Charged-Particle and Neutron Multiplicity Measurements

D.G. Sarantites, T.M. Semkow, L.G. Sobotka,
V. Abenante, Z. Li, Z. Majka, N.G. Nicolis, and D.W. Stracener
Department of Chemistry, Washington University, St. Louis, Missouri 63130

D.C. Hensley and J.R. Beene
Oak Ridge National Laboratory, Oak Ridge, Tennessee 37830

and

H.C. Griffin
University of Michigan, Ann Arbor, Michigan 48109

ABSTRACT

We have studied the excitation of target-like fragments produced in the reactions of 331.9 MeV ^{28}Si + ^{181}Ta The light charged particles and intermediate mass fragments were detected in a small, highly segmented 4π phoswich detector system placed inside the spin spectrometer, a 4π NaI array which served as a neutron and γ-ray detector. All target emissions indicate that excitation ceases to increase with decreasing projectile-like fragment energy, as it should if the primary reaction is binary. Non-equilibrium neutron, proton and α-particle emission and projectile fragmentation conspire and limit the conversion of kinetic energy into target excitation. This effect is more pronounced for PLF away from the injection point and for the largest kinetic energy losses.

1. INTRODUCTION

When the relative velocity of two heavy ions at contact exceeds approximately 3 cm/ns, complete fusion of the projectile and target begins to yield cross section to other less than complete fusion mechanisms.[1-4] These mechanisms are often characterized by less than full momentum transfer, and imply the existence of prompt emission of unfused nucleons, or an unfused projectile (or target) remnant, or both. In each case, the incomplete momentum transfer results in both lower velocity and excitation energy of the products relative to those from complete fusion. The extent of momentum transfer manifested in fragment velocities has been extensively studied by direct measurement of the recoil velocity of fusion-like products and for fissile systems by the folding angle technique. While such measurements have been very important in the study of incomplete fusion, they cannot by themselves distinguish between mechanisms. More recently, neutron

multiplicity measurements have shown that target excitation provides information similar to that of the velocity measurements.[5] Again, these measurements by themselves are insufficient to answer the question whether the reduction in momentum transfer is due to fast light particle emission, or to an unfocused part of the projectile or both.

The purpose of the present work is to distinguish between these possibilities. We have addressed these questions by means of a complete 4π measurement of the light charged particles, light intermediate fragments, neutrons and γ-rays observed simultaneously in coincidence with projectile-like fragments. We will show that for an appropriate choice of the reaction system, it is possible to kinematically decompose the energy spectra into those due to sequential emission from the target-like fragment (TLF), the projectile-like fragment (PLF), and a fast forward component (FC). We will show that the deficit in TLF excitation which is not associated with a projectile remnant strongly depends on both the mass and the energy of the residual projectile-like fragment.

2. EXPERIMENTAL METHODS

The experiments in this work were performed at the Holifield Heavy-Ion Research facility. A 331.9 MeV (11.85 MeV/nucleon) ^{28}Si was used to bombard $\sim$ 500 μg/cm^2 self supporting ^{181}Ta targets. The proton , α-particle and Li and some Be spectra were recorded in the "Dwarf Ball", a 4π light-charged particle spectrometer system. It consists of 72 fast-slow particle scintillator phoswiches closely packed in a 4π arrangement. A detailed description of this apparatus has been given in Ref. 6. Each telescope of the Dwarf Ball covered 0.171 radians. The Dwarf Ball was placed inside the spherical scattering chamber of the spin spectrometer.[7] The NaI detectors of the spin spectrometer provided the γ-ray multiplicity, the total γ-ray energy and the neutron multiplicity. The response of the spin spectrometer to monoenergetic neutrons was determined via the ^{7}Li(p,nγ)^{7}Be reaction[7] and was further checked with the (^{20}Ne,6nγ) reaction. The event triggering efficiency Ω_T varies between 0.55 and 0.40 for 2 to 16 MeV neutrons, while the fold triggering efficiency Ω_T(1+F), which includes the crystal-to-crystal scattering, varies between 0.95 and 1.20 for neutron spectra[7] with a Boltzmann distribution with temperatures between 1 and 4 MeV, respectively.

The event triggers were provided by three Si (ΔE, E) telescopes consisting of 45 μm ΔE, and 1500 μm E detectors with an active area of 200 mm^2, subtending

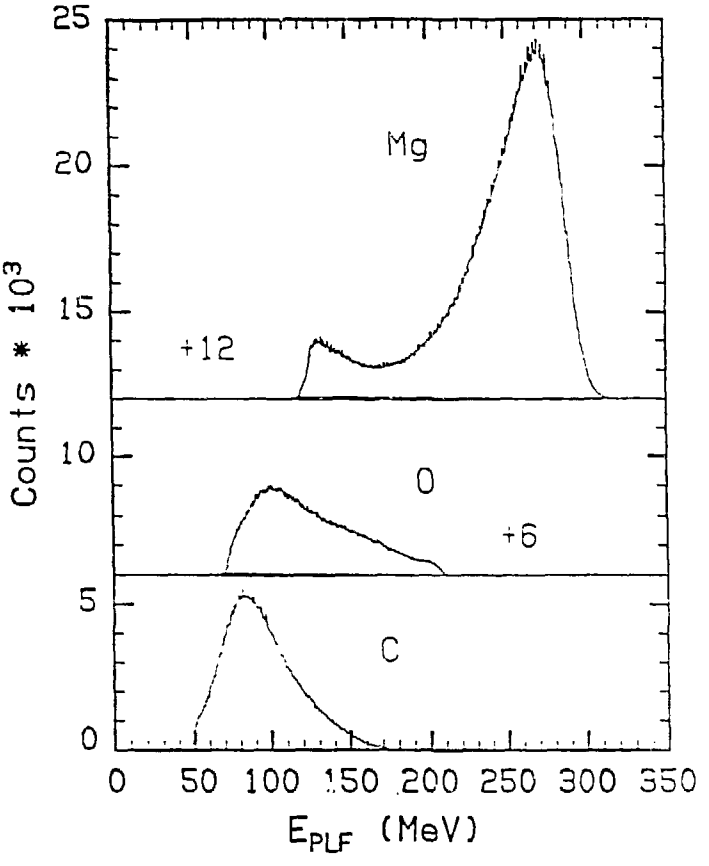

Figure 1. Kinetic energy spectra for all the isotopes of C, O, and Mg PLF recorded by the triggering Si telescopes at 27.1° to the beam direction. The quasielastic component is seen strong in the Mg spectrum, but it is absent in the C spectrum.

~10 mstr each. Two of these telescopes were located at 27.1° to the beam direction, while a third one was placed at 102° to monitor the α-particle spectra with good energy resolution.

3. RESULTS AND DISCUSSION

Energy spectra of the PLF were recorded in the two forward Si telescopes for all Z values ranging from Li to Si. Mass and Z resolution was obtained for all elements from Li to Mg. The energy spectra for Z=14 down to 10 exhibited both the quasielastic and the fully relaxed (deeply inelastic) component with the latter increasing in strength as one moves away from the injection point. Selected PLF kinetic energy spectra for all the C, O and Mg isotopes are shown in Fig. 1. The coincident light particle spectra were obtained by placing 5 or 7 approximately equal width gates on the PLF energy spectra during the analysis.

The excitation energy deposited in the TLF as a function of energy loss and Z of the PLF was obtained from the neutron, proton and α-particle multiplicities when these light particles are emitted in the backward direction from the slowly moving target-like products. The neutron multiplicity from the TLF is best determined from the total neutron multiplicities and the angular distributions of the neutron events recorded in the spin spectrometer. The neutron-fold distributions in coincidence with the Mg, O and C fragments are shown in Fig. 2(a)-(c), for the indicated PLF energies. Several features are apparent in these data. First, we note that in the Mg case, the neutron fold distributions shift continuously toward higher multiplicities as the Mg kinetic decreases. This is in contrast with the O and C cases where a saturation effect is apparent. As the observed kinetic energy is decreased and thus more energy is available for heating the system, the total neutron multiplicities first increase and then remain constant, suggesting that additional kinetic energy loss is not utilized to heat the reaction products. Another feature of the neutron fold distributions is their large widths. Although a significant fraction of the width is due to the instrumental response of the spin spectrometer[7] from the rather large crystal-to-crystal scattering of the neutrons, still the present data indicate rather large widths of the neutron multiplicity distribution.

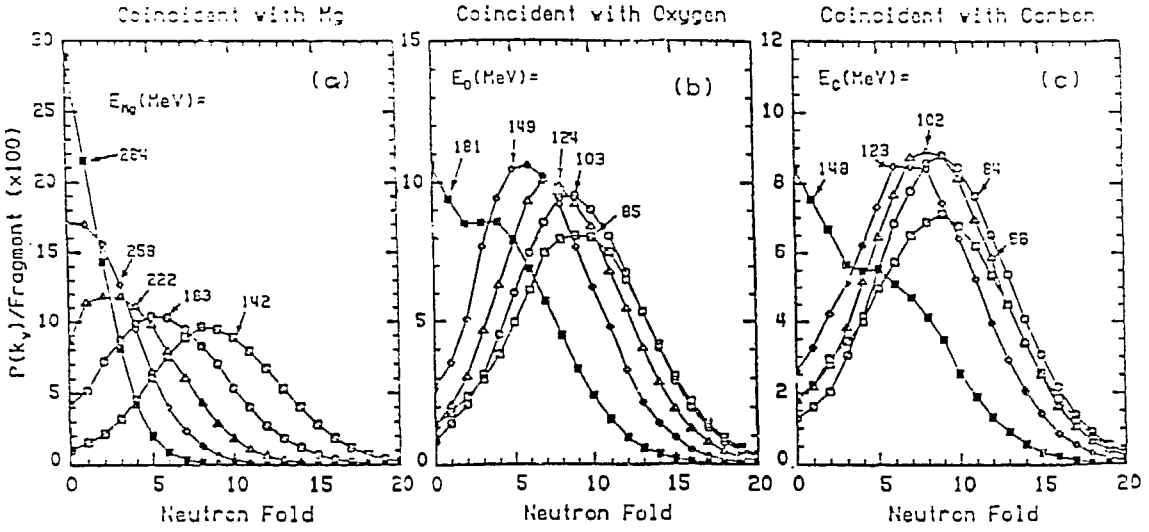

Figure 2. Total neutron fold distributions observed in the spin spectrometer in coincidence (a) with Mg fragments having the indicated average kinetic energies, (b) with O fragments having the indicated average kinetic energies, and (c) with C fragments having the indicated energies.

The average total neutron multiplicities $\langle M_n \rangle_{tot}$, were calculated from the average neutron fold distributions corrected for instrumental response. The results are summarized in column 2 of the Table I as a function of E_{PLF} for Mg, O and C fragments. The neutron multiplicities for the TLF can be obtained from the $\langle M_n \rangle_{tot}$, by making use of the kinematic focusing of the neutrons due to the fast moving PLF or the fast forward component from those emitted from the heavy slowly moving TLF. An example of such an angular distribution is shown in Fig. 3 for neutrons observed in coincidence with 222 MeV Mg fragments. The distribution is plotted with respect to the angle of the Mg fragment, although a similar plot is obtained relative to the beam direction. The resolution of such distributions into a target-like component and a forward component can be made with the aid of a simulation that takes into account the appropriate kinematic parameters. This is shown in Fig. 3 by the solid line. The forward neutron multiplicity contains both the PLF and any fast forward neutrons which cannot be resolved from each other due to the large crystal-to-crystal scattering of the energetic neutrons. The average neutron multiplicities for the target-like component, $\langle M_n \rangle_{TLF}$, were obtained from $\langle M_n \rangle_{tot}$, using the appropriate fractions for the TLF deduced from the angular distributions. The results are given in column 3 of Table I.

Before discussing the relationship between neutron multiplicity and excitation energy, we will discuss the charged particle multiplicities from the various sources of emission. We note first that the total proton and α multiplicities for all exit channels from this reaction are less than unity. In order to decompose the ensemble of spectra from all the detectors of the Dwarf Ball, it is instructive to distinguish two classes of events. First, we consider events that are not accompanied by a non-equilibrium particle. Then the PLF has a known direction and velocity and the associated sequentially emitted light particle will be focussed kinematially in a known way. Assuming that the moving source (primary PLF) emits the particle after leaving the interaction zone, we can approximate the spectra with Boltzmann-like distributions in the source rest frame with a Coulomb barrier, V_{Coul}, moving with the source energy ε_S. Then the differential cross section in the laboratory is written:

$$\left(\frac{d^2\sigma}{d\Omega dE}\right)_L = \frac{M}{4\pi T^2}\sqrt{\frac{E_L}{E_{CM}}}\,(E_{CM} - V_{Coul})\; e^{-(E_{CM}-V_{Coul})/T} \qquad (1)$$

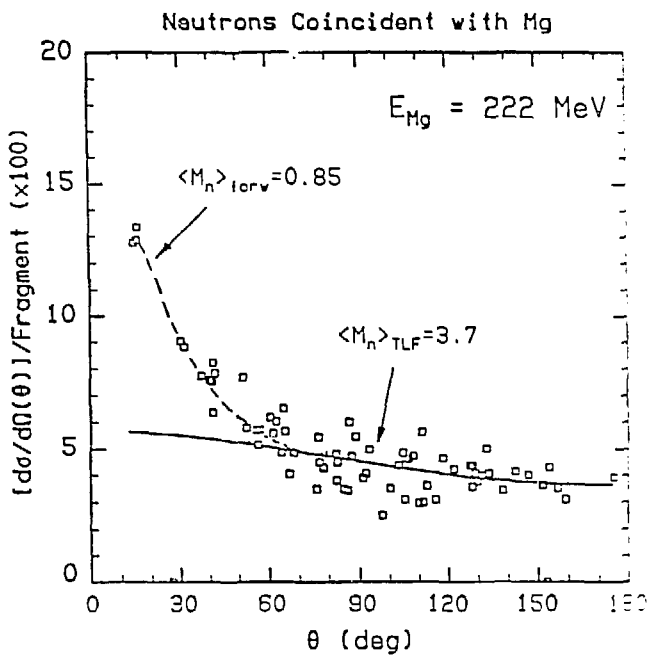

Figure 3. An example of an angular distribution of neutrons observed in the spin spectrometer in coincidence with 222 MeV Mg fragments. The angles are relative to that of the Mg. Two components are clearly seen. The forward peaked component arrives from both the sequential decay of the PLF and the fast non-equilibrium of neutrons. The large crystal-to-crystal scattering prevents the resolution of these two components. The smaller forward focusing due to the slowly moving TLF is clearly seen.

where M is the multiplicity, E_L is the observed light particle laboratory energy, the center-of-mass energy $E_{CM} = \mu v_{rel}^2/2$ with $v_{rel}^2 = v^2 + v_{PLF}^2 - 2vv_{PLF}\cos\theta$, with $\mu = (m_{PLF} \cdot m)/(m_{PLF} + m)$, m and v are the mass and velocity of the light particle, m_{PLF} and v_{PLF} are the mass and speed of the detected PLF, θ is the angle between the secondary PLF and the light particle, and T is the temperature parameter for the sequential emission. We note that Eq. (1) includes the recoil correction due to emission of the light particle, which in the case of an α-particle, is significant. The emission from the TLF is also well characterized in this case and Eq. (1) still applies, but now the primary v'_{TLF} is calculated from binary kinematics and $v_{rel} = v_1 + v_2$ with $v_1^2 = v^2 + v'^2_{TLF} - 2vv'_{TLF}\cos\theta'$, $v_2 = v_1 m_P/m_{TLF}$ and $E_{CM} = \mu v_{rel}^2/2$ as before.

Next we consider the case where a non-equilibrium emission preceeds the binary decay. In this case, the emission of the non-equilibrium particles must be described by kinematics appropriate to the mechanism that produces them. We have adopted a parameterization that assumes emission centered along the beam

Table I. Multiplicities of protons and neutrons emitted from the TLF in the reactions of 331.9 MeV ^{28}Si + ^{181}Ta leading to Mg, O, and C PLF. Deduced TLF excitation energies are also given.

E_{Lab} (MeV)	$\langle M_n \rangle_{tot}$	$\langle M_n \rangle_{TLF}$	$\langle E^*_{TLF} \rangle_n$ (MeV)	$\langle M_p \rangle_{TLF}$	$\langle E^*_{TLF} \rangle_p$ (MeV)	$\langle E^*_{TLF} \rangle$ (MeV)
E_{Mg}						
142	9.77 20	8.69 20	113 4	0.258 10	115 4	114 3
183	6.55 15	5.59 15	67 3	0.073 3	76 3	72 3
222	4.57 10	3.72 10	43 2	0.0185 8	49 3	46 2
258	2.73 10	2.36 10	28 2	0.0096 4	–	28 2
284	1.47 8	1.36 9	17 2	0.0070 5	–	17 1
E_O						
85	9.57 20	8.64 20	117 3	0.256 10	103 3	110 5
103	9.41 20	8.33 20	112 3	0.242 10	101 3	107 5
124	8.33 20	7.11 20	93 3	0.176 8	90 3	92 3
149	7.07 18	5.88 18	74 3	0.094 5	75 3	75 3
181	4.85 12	4.17 12	52 2	0.035 2	54 2	53 2
E_C						
66	8.49 20	6.8 2	96 3	0.230 10	94 3	95 3
84	8.90 20	7.7 2	112 5	0.265 9	98 4	105 6
102	8.22 18	7.2 2	103 6	0.199 8	90 4	96 5
129	7.08 16	6.2 2	86 5	0.126 6	76 4	81 4
148	4.76 14	4.4 1	59 3	0.062 5	61 3	60 2

direction from a moving source of energy ε_S, but with a Coulomb barrier moving much more slowly because of the heavy system at hand. In this case the differential cross section is:

$$\left(\frac{d^2\sigma}{d\Omega dE}\right)_L = \frac{M}{4\pi T^2}\sqrt{(E_L - V_{Coul})E_{CM}} \cdot e^{-E_{CM}/T} \qquad (2)$$

$$\text{with } E_{CM} = (E_L - V_{Coul}) + \varepsilon_S - 2 \cdot \sqrt{(E_L - V_{Coul})\varepsilon_S} \cdot \cos\theta.$$

Now the emission of non-equilibrium particles alters the energy balance for the decay of the remaining composite system. However, Eq. (1) is still applicable for the PLF emission because v, v_{PLF}, and θ are still known from the measurement. For the TLF the situation is different. Here we do not measure the TLF and we must rely on energy and momentum conservation to obtain v'_{TLF}. In view of the large asymmetry of the entrance and exit channels in this reaction, we find that $v_{TLF} \leq 0.5$ cm/ns, which is typically less than 15% of the PLF velocity. Consequently, we can show that the error introduced by assuming binary kinematics does not influence significantly the deduced TLF particle multiplicities.

Selected spectra of protons and α-particles are shown in Figs. 4(a) and 4(b). These were recorded at the angles indicated in coincidence with 103 MeV O and 66 MeV C fragments. The solid lines are global fits to the backward hemisphere using Eq. (1) for the TLF as discussed above.

As it was mentioned earlier, the proton spectra observed in coincidence with the PLF clearly exhibit three components. Two of these are easily ascribed to the sequential emission from the PLF and TLF as evidenced by the observed kinematic focusing. The third component is peaked along the beam direction and does not seem to have a marked in- and out-of-plane correlation. Using the procedure described earlier, we have fitted the proton energy spectra with three components. The two components describing the sequential emission were taken as a linear combination of two terms given by Eq. (1) and the third forward component was described by Eq. (2). The results of the fits with this decomposition are shown in Fig. 5.

The full circles correspond to the proton emission from the TLF, and squares give the emission from the PLF and the diamonds correspond to the forward component. These average proton multiplicities are plotted as functions of the available energy $E_{avail} = E_{proj} - E_{PLF}$ without any Q_{gg} term. We note that for the triggering fragments near the projectile such as Mg, the proton multiplicity from the TLF increases rapidly with available energy in contrast to that from the PLF, which is essentially constant and for the highest E_{avail} appears to decrease somewhat. On the other hand, the beam direction component also remains constant until the highest available energy bin at which point it shows an increase. As the detected

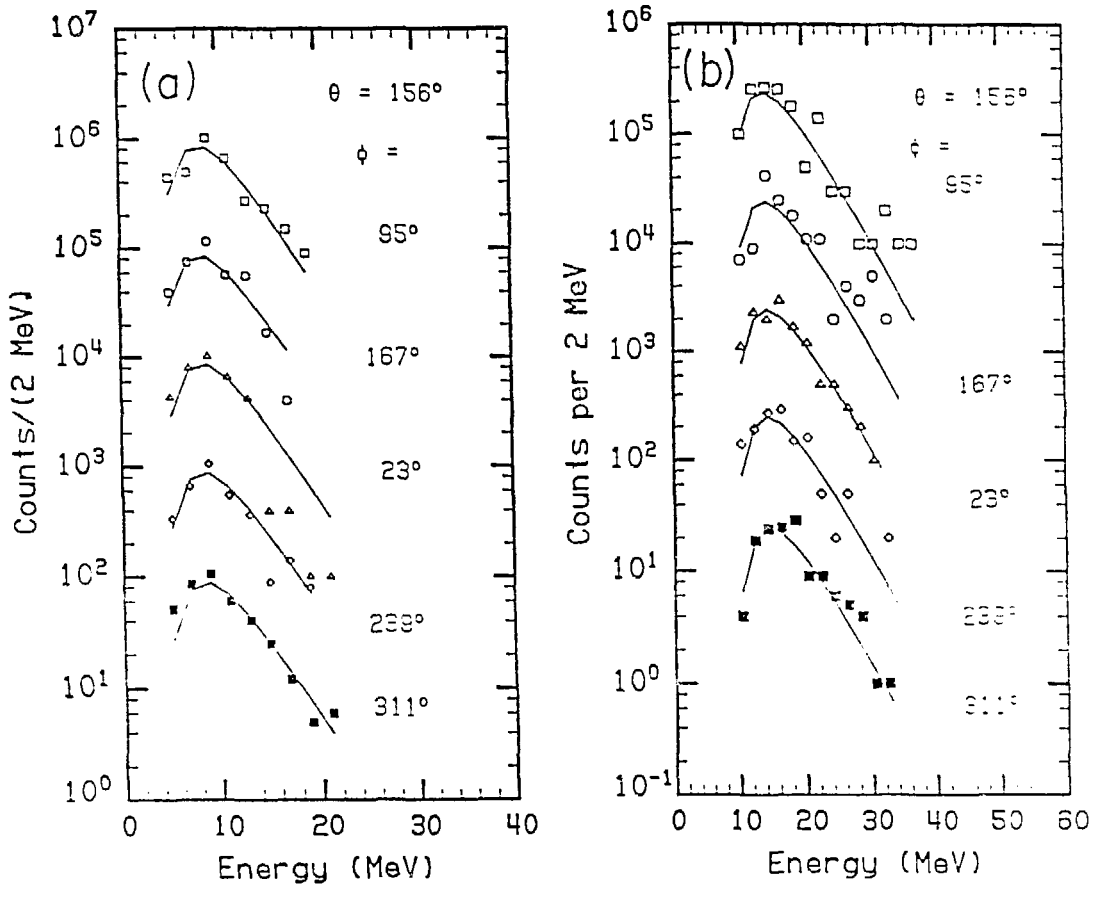

Figure 4. (a) Proton energy spectra recorded at the most backward ring of detectors of the Dwarf Ball at the indicated angles observed in coincidence with 103 MeV O fragments. The solid lines give the global fits to Eq. (1) with the parameters $v_O = 0.45$ cm/ns, $T = 2.6 \pm 0.1$ MeV, and $M_p = 0.24 \pm 0.01$. (b) Alpha-particle spectra recorded in coincidence with 66 MeV C fragments at the indicated angles. The solid lines are global fits to Eq. (1) with the parameters $v_C = 0.51$ cm/ns, $T = 3.1 \pm 0.1$ MeV and $M_\alpha = 0.083 \pm 0.003$.

PLF moves further away from the projectile, a different behavior is observed. Now the M_p values from the TLF first increase with E_{avail} but then they level off (see the oxygen data in Fig. 5) and for the events coincident with C they even show a decrease. In contrast, the M_p from the PLF shows a continuing increase with E_{avail} which becomes even more pronounced as we move from the O to the C detected fragments. A similar pattern is observed for the multiplicity of the beam direction component, which shows a continuing increase with E_{avail} that becomes stronger in going from the O to the C detected fragments.

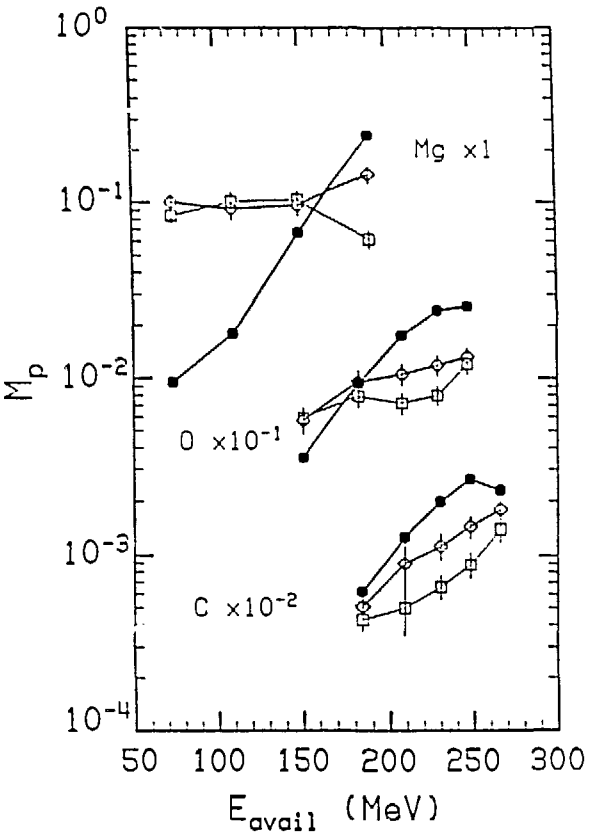

Figure 5. Average proton multiplicities from the TLF (full circles), the PLF (open squares), and the beam direction component (open diamonds) as functions of the available energy $E_{avail} = E_{proj} - E_{PLF}$ for Mg, O, and C detected fragments. The multiplicities coincident with O and C are scaled down by factors of 10 and 100, respectively.

We note here that the above results for the proton multiplicities are consistent with the neutron multiplicities discussed earlier. The results presented in Fig. 5 provide evidence for the energy sharing between the binary fragments under the influence of faster mechanisms responsible for the emission of the beam-direction particles.

We proceed next to convert the particle multiplicities to fragment excitation. For this purpose, we need to know the primary Z and A of each fragment and the average mass, charge and energy removed by the fast beam-direction component. With the complete set of data acquired with the 4π measurement, this can be done by decomposing the spectra from the various "exit channels" associated with 1p, 2p, 1α, 1α1p, 1α2p, 2α, 2α1p, etc. emission from all sources into their respective

components. We are in the process of doing this in detail. Here we will discuss the excitation of the TLF which can be deduced rather easily.

We first turn our attention to the events associated with the Mg fragments. From first glance, the M_p results in Fig. 5 and the $\langle M_n \rangle_{TLF}$ values in Table I show that the TLF gains excitation rapidly with increasing E_{avail} whereas the PLF appears to have constant excitation which may decrease somewhat at the highest E_{avail}. At the same time, a small rather slowly increasing amount of energy is attributed to the beam direction component (note that $\langle M_p \rangle_{FC} \sim 0.1$). This picture is corroborated by examining the probability per fragment for evaporation of mass associated with charged particle emission for various values of E_{Mg} as shown in Fig. 6.

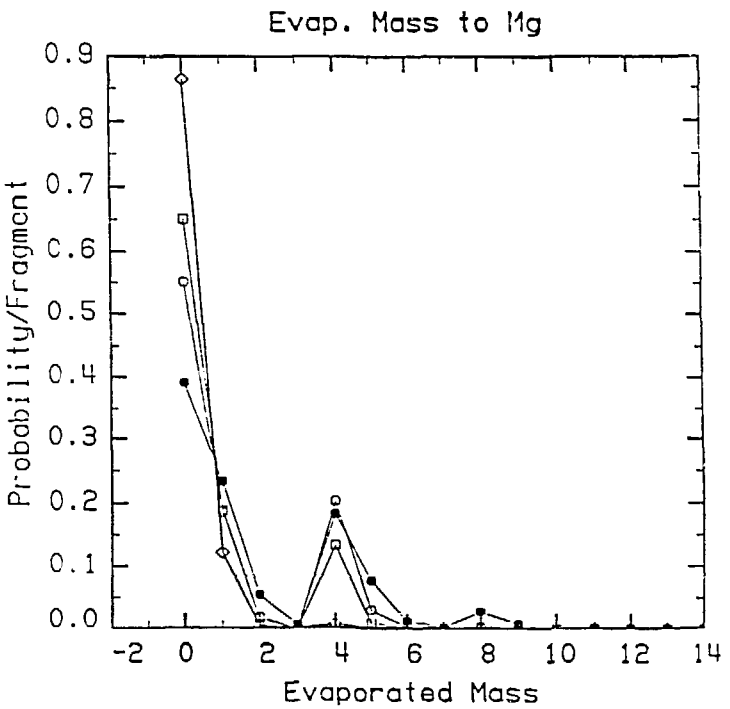

Figure 6. Probability distributions per detected Mg fragment of the evaporated mass from all sources for four values of E_{avail}: 38 MeV (diamonds), 87 MeV (squares), 142 MeV (open circles), and 197 MeV (full circles).

For the lowest available energy (near the quasielastic peak) practically only one proton can be emitted. As the available energy is increased from 38 to 87 MeV, the 1p probability increases somewhat, but a sudden jump in α emission is seen. Further increases in E_{avail} gives a smooth increase in proton and in α multiplicity, but only at the highest E_{avail} some 2α emission is seen. These results

indicate that for the Mg detected fragments, the primary fragments do not change in Z and A appreciably with increasing E_{avail} for the last three energy bins. In this case, one can identify the primary TLF and use evaporation calculations for TLF fragments at different excitations in order to relate the $\langle M_n \rangle_{TLF}$, and $\langle M_p \rangle_{TLF}$ with excitation energy. This is shown in Fig. 7 where the neutron and proton multiplicities are shown. These were calculated with the statistical model code CASCADE[8] using an initial spin value of 15 $\hbar$. The (Z, A) values for the primary TLF were obtained assuming the following partitions $^{25}Mg + {}^{184}Re$, $^{17}O + {}^{192}Au$ and $^{13}C + {}^{196}Tl$ for the proton emission, and $^{25}Al + {}^{184}Hg$, $^{18}F + {}^{191}Pt$, and the average of $^{13}C + {}^{196}Tl$ and $^{13}N + {}^{196}Hg$ for the neutron emission.

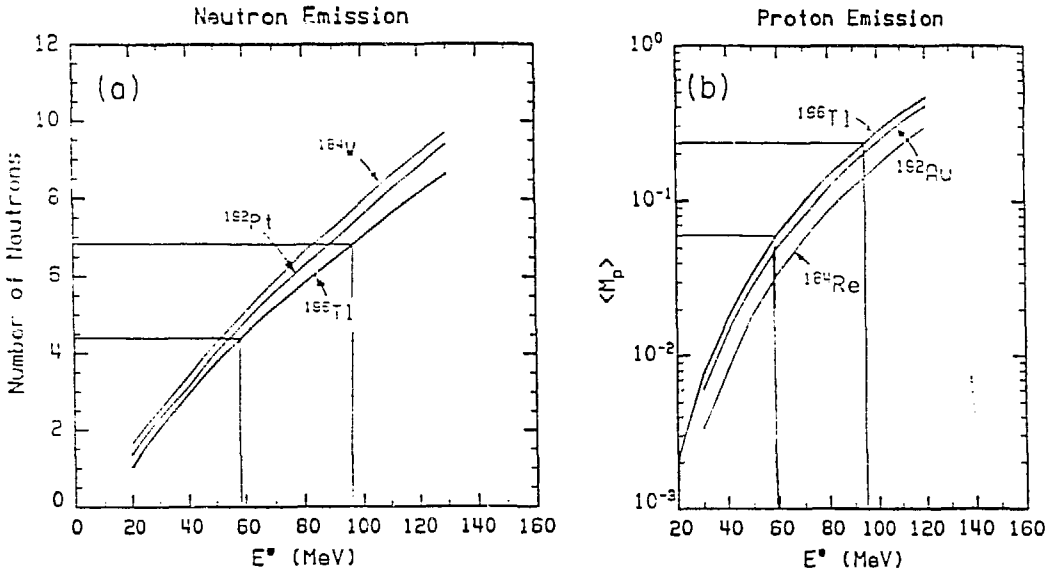

Figure 7. (a) Calculated average neutron multiplicities as a function of excitation energy in the indicated TLF taken to be $^{25}Al + {}^{184}Hg$ for the Mg triggers, $^{18}F + {}^{191}Pt$ for the O triggers, and $^{13}C + {}^{196}Tl$ for the C triggers. (b) Calculated average proton multiplicities as a function of excitation energy in the indicated TLF taken to be $^{25}Mg + {}^{184}Re$, $^{17}O + {}^{192}Au$, and $^{13} + {}^{196}Tl$ for the Mg, O, and C triggers, respectively. The vertical and horizontal lines indicate that similar excitation energies are deduced either from the proton or neutron multiplicities. The examples are for $E_c = 66$ and 129 MeV (see also Table I).

At first glance, the results shown in Table I for the Mg case imply a continuing increase in TLF excitation with increasing E_{avail}, whereas for the O and C fragments, the observed saturation in M_p implies a limitation of excitation of the TLF as the E_{avail} is increased.

There are three important processes or factors that can influence the above mentioned conclusions. These are (1) fission or heavy fragment emission from the TLF, (2) a drift in the average primary PLF charge and mass to heavier fragments closer to the projectile as the energy of the detected PLF is decreased, and (3) emission of fast non-equilibrium light charged particles and neutrons and projectile fragmentation. Clearly, all these processes are present to some extent and it will be our task to evaluate their relative importance both as a function of exit channel Z and E_{avail}.

Considering the first factor, we note that intermediate fragment emission from the TLF is very small. Fission, on the other hand, acquires significant cross section (up to ~30%) for the highest E_{avail} values in the case where C fragments were the triggers. The effect of fission, however, is to increase somewhat the neutron multiplicity and decrease the charged particle multiplicity by a small amount, compared to light particle emission from the initial TLF. Although the presence of fission alters the kinematics, a proper account of this would not alter the present conclusions significantly.

Since the charged particle multiplicity (see Fig. 5) in coincidence with Mg fragments is essentially constant we can assume that the primary PLF associated with the Mg fragment does not change with E_{avail}. In Fig. 8, we show plots of the fractions of $(E^*)_{TLF}$ and $(E^*)_{TLF}/E^*_{total,\ 2body}$ as functions of E_{avail} and $E^*_{total,\ 2body}$, respectively. The sharp rise of the fraction of energy going into the target excitation is quite apparent for the Mg triggers. If the same analysis is made for the target excitation for the O and C triggers, a different picture appears. Here a less rapid increase of the target excitation with increasing E_{avail} is seen, which is followed by a decrease in the case of C. Figure 8(b) shows the fraction of excitation carried by the TLF if only binary decay is assumed. For the Mg PLF, a maximum of ~71% is reached, while considerably lower fractions are found for all values of $E^*_{total,\ 2body}$.

We now focus on the influence of the second factor on the target excitation. A drift in the average primary PLF mass may occur as the observed PLF kinetic energy is varied. At the onset, we can see that as the E_{avail} is increased for a given detected PLF, say C, the primary fragment may have higher Z and A and this will cause the TLF to have correspondingly smaller Z and A. This effect will result in a somewhat higher deduced excitation for a given $\langle M_p \rangle$ or $\langle M_\alpha \rangle$ [see Fig. 7(b)], but it will give somewhat lower target excitation for the same neutron multiplicity

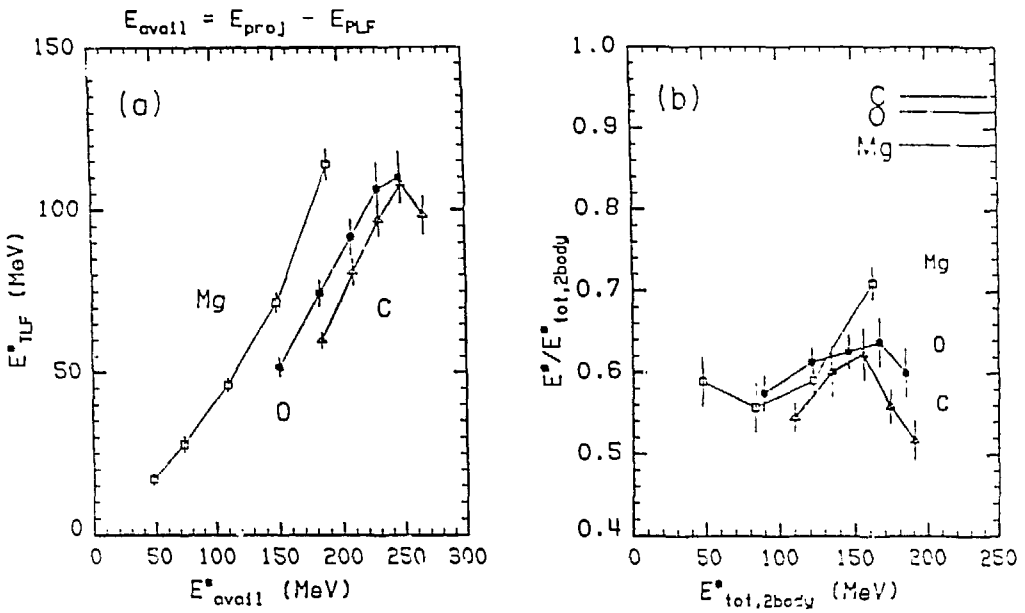

Figure 8. (a) Deduced TLF excitation as a function of $E_{avail} = E_{proj} - E_{PLF}$ for Mg, O and C PLF triggers. Note the different rate of conversion of available energy into target excitation and the leveling off of O and decrease for C PLF. (b) Calculated fraction of TLF excitation as a function of total available energy assuming a binary division.

$\langle M_n \rangle$ [see Fig. 7(a)]. If carried out quantitatively, this procedure may improve the agreement of excitation energies deduced for $\langle M_n \rangle$ and $\langle M_p \rangle$ data in Table 1, but it cannot significantly alter our conclusions. To see this in more detail, we refer to Figs. 5 and 6 for the Mg PLF. In this case we have already argued that the mass of the PLF does not change significantly with E_{Mg} at least for the three highest E_{avail} bins.

Next, we examine in some detail the C fragment triggers. In Fig. 9, we show the total evaporated mass of charged particles from all sources. It is seen that as E_C decreases (E_{avail} increases) a drift to higher evaporated masses is observed. We have looked at this further by examining the differential multiplicity of proton and α emission in the detectors adjacent to the Si (Δ E, E) telescope for 1p, 2p, 3p, 1α, 1α1p, 1α2p, 1α3p, and 2α as a function of E_C. A definite and systematic drift was easily identified in this case. We estimated, however, that this effect will not alter significantly the saturation in target excitation observed. This leaves, therefore, the third alternative as the cause of the limited conversion of kinetic energy to target excitation, i.e. the emission of fast particles along the beam direction which

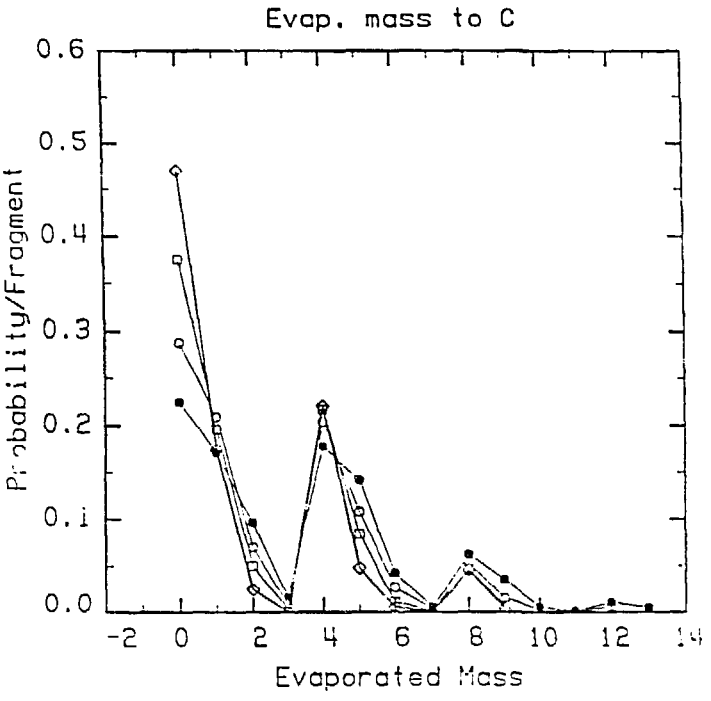

Figure 9. Probability distributions per detected C fragment of the evaporated mass from all emitted sources for four values of E_{avail}: 182 MeV (diamonds), 214 MeV (squares), 241 MeV (open circles), 270 MeV (full circles).

remove some of the available energy for channels far from the entry point and for the large kinetic energy losses.

We have pursued this matter further in order to characterize the relative importance of the beam direction particles and their influence on the energy balance of the remaining TLF and PLF.

There are four types of particles that conspire to reduce the available energy for excitation of the target and projectile-like fragments. These are fast neutrons, protons, α-particles, and intermediate mass fragments. We have evidence indicating that the importance of such emissions is exit channel dependent, and that for PLF far from the injection point, they depend on the available energy for exciting the system.

We have already presented evidence for proton emission along the beam direction (Fig. 5). Similar results are obtained from the analysis of angular distributions of α spectra. We find that for C detected fragments, the partitions in which only 1α or 2α, or $1\alpha 1p$ are emitted provide the largest forward peaked α multiplicities. The observed neutron angular distribution also supports the emission of fast forward neutrons. In Fig. 10 we show the average multiplicity of

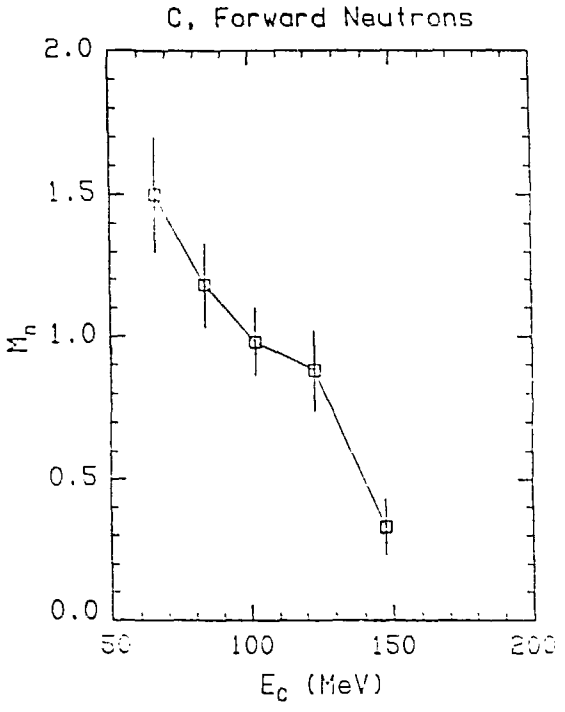

Figure 10. Average forward neutron multiplicity observed in coincidence with C fragments as a function of the detected C energy.

neutrons emitted in the forward direction as a function of the detected C energy. Although we cannot experimentally distinguish between the fast and the forward sequentially emitted neutrons from the PLF, we find that the increase in the forward neutrons with decreasing PLF energy is strong only for C and not in O or Mg (see Table I).

We have also obtained evidence from correlated coincidence measurements that for the triggers such as C, and others far from the injection point, there is emission of Li and possibly other intermediate fragments. These are emitted along the beam direction and they are not focused in the direction of the detected PLF. Furthermore, the production of these intermediate fragments increases in importance as the kinetic energy loss increases. This is associated with projectile fragmentation which occurs at this bombardment energy and contributes in a significant amount to the production of the lighter detected PLF with the lowest observed kinetic energies.

Thus we conclude that forward emission of light particles from non-equilibrium processes and of intermediate fragments from projectile fragmentation

conspire to limit the excitation of the target like products for ejectiles far from the projectile and for the largest values of the kinetic energy loss.

The above conclusions can be made quantitative if the primary (Z, A) distributions from the PLF and TLF are determined for each detected PLF energy bin in conjunction with average M_n, M_p, M_α, M_{Li}, etc. and their respective energies of the fast forward emitted particles. This can be done if the 4π nature of this experiment is utilized. For example, referring to Fig. 3, we can resolve the proton and α-particle spectra from each reaction type, (ie. only 1p, 2p, 3p, 1α, 1α1p, etc. emissions) into the TLF and PLF sequential components and the forward peaked components. This information, in conjunction with the associated neutron multiplicity and the higher order correlations in the case of multiple particle emission, will give the ensemble of nuclei that lead to the detected PLF and its TLF partner. We are currently in the process of doing this.

References

1. H. Morgenstern, W. Bohne, W. Galster, K. Grabisch, and A. Kyanowski, *Phys. Rev. Lett.* 52, 1104 (1984).
2. Y. Chan, C. Albiston, M. Bantel, A. Budzanowski, D. DiGregorio, R.G. Stokstad, S. Wald, S. Zhou, Z. Zhou, Proceeding of the Symposium on the Many Facets of Heavy-Ion Fusion Reactions, Argonne National Laboratory, ANL-Phy-86-1.
3. A.S. Goldhaber, *Phys. Lett.* 53B, 306 (1974).
4. W.A. Friedman, *Phys. Rev.* C27, 569 (1983).
5. U. Jahnke, G. Ingold, D. Hilscher, M. Lehmann, E. Schwinn, and P. Zank, *Phys. Rev. Lett.* 57, 190 (1986).
6. D.G. Sarantites, L.G. Sobotka, T.M. Semkow, V. Abenante, J. Elson, J.T. Hood, Z. Li, N.G. Nicolis, D.W. Stracener, and J. Valdes, *Nucl. Instr. and Meth.* (in press).
7. M. Jääskeläinen, D.G. Sarantites, R. Woodward, F.A. Dilmanian, J.T. Hood, R. Jääskeläinen, D.C. Hensley, M.L. Halbert, and J.H. Barker, *Nucl. Instr. and Meth.* 204, 385 (1983); and T.M. Semkow, D.G. Sarantites, V. Abenante, Z. Li, and L.G. Sobotka, to be published.
8. F. Puhlhofer, *Nucl. Phys.* A280, 267 (1977).